

# Microstructure and Mechanical Properties of Laves Phase-strengthened Fe-Cr-Zr Alloys

L. TAN and Y. YANG

Laves phase-reinforced alloys have shown some preliminary promising performance at room temperatures. This work aims at evaluating mechanical properties of Laves phase-strengthened alloys at elevated temperatures. Three Fe-Cr-Zr alloys were designed to favor the formation of eutectic microstructures containing Laves and body-centered cubic phases with the aid of thermodynamic calculations. Microstructural characterization was carried out on the alloys in as-processed and aged states using optical microscopy, scanning electron microscopy, energy-dispersive X-ray spectroscopy, and X-ray diffraction. The effect of thermal aging and alloy composition on microstructure has been discussed based on microstructural characterization results. Mechanical properties have been evaluated by means of Vickers microhardness measurements, tensile testing at temperatures up to 973.15 K (700.15 °C), and creep testing at 873.15 K (600.15 °C) and 260 MPa. Alloys close to the eutectic composition show significantly superior strength and creep resistance compared to P92. However, their low tensile ductility may limit their applications at relatively low temperatures.

DOI: 10.1007/s11661-014-2695-1

© The Minerals, Metals & Materials Society and ASM International (outside the USA) 2014

## I. INTRODUCTION

ADVANCED structural materials with excellent high-temperature strength and resistance to thermal creep, corrosion, and neutron irradiation are essential for advanced reactors with enhanced safety margins, design flexibility, and economics. High-Cr (9 to 12 wt pct) ferritic-martensitic (FM) steels are important structural materials for nuclear reactors due to their advantages over other applicable materials like austenitic stainless steels in face-centered cubic (fcc) structure, notably for their resistance to void swelling, low thermal expansion coefficients, and higher thermal conductivity.<sup>[1–3]</sup> Their superior radiation resistance is primarily due to the body-centered cubic (bcc) structure of the matrix as reviewed by Raj *et al.*<sup>[3]</sup> However, current FM steels are not qualified for applications at temperatures above 893.15 K to 923.15 K (620.15 to 650.15 °C) because they suffer significant strength reduction once beyond the temperatures and approaching the bcc–fcc transformation temperature.<sup>[4,5]</sup> Alloys with full bcc structure by eliminating the bcc–fcc transformation would be able to prevent such strength reduction and thus be allowable for use at higher temperatures.

Laves phases are among potential intermetallic compounds being considered as strengthening elements for high-temperature structural alloys.<sup>[6–8]</sup> Room-temperature mechanical properties have been investigated in both Fe-Zr binary and Fe-Cr-Zr ternary alloys with

Laves phase as a strengthening element.<sup>[9–11]</sup> A significant strengthening effect of Laves phase was observed in an Fe<sub>90</sub>Zr<sub>10</sub> alloy at room temperature, *e.g.*, compression yield strength/plastic strain of 2.2 GPa/1.5 pct.<sup>[9]</sup> All compositions throughout the article are stated in at. pct. A slower cooling rate led to a lower strength but noticeably increased plastic strain of 1.9 GPa/9 pct at room temperature.<sup>[10]</sup> Room-temperature plastic strain could also be improved by changing alloy composition. Reducing Zr to Fe<sub>94</sub>Zr<sub>6</sub> led to a remarkable increase in plastic strain compensated with some reduction in strength as 1.5 GPa/12 pct.<sup>[9]</sup> In contrast to the nearly 100 pct fine eutectic microstructure in Fe<sub>90</sub>Zr<sub>10</sub>, the Fe<sub>94</sub>Zr<sub>6</sub> alloy contains fine eutectic microstructure and coarse primary bcc (Fe) phase. Partial substitution of Fe with Cr while keeping constant Zr content also enhanced the room-temperature plastic strain, *e.g.*, Fe<sub>80</sub>Cr<sub>10</sub>Zr<sub>10</sub> with 2.13 GPa/17 pct.<sup>[11]</sup> The enhanced ductility was attributed to the formation of Cr-stabilized C14 Laves. However, the knowledge on high-temperature mechanical properties of the Fe-Cr-Zr alloy is currently not available. This work investigates the temperature-dependent tensile properties and high-temperature creep strength of carefully designed Fe-Cr-Zr alloys in both as-processed and isothermally aged conditions, providing insights on their potential applications as high-temperature structural materials.

## II. EXPERIMENT

### A. Alloy Design and Processing

Three Fe-Cr-Zr alloys were designed in this work. The design of alloy A1 started with the Fe<sub>80</sub>Cr<sub>10</sub>Zr<sub>10</sub> composition proposed by Scudino *et al.*,<sup>[11]</sup> as it exhib-

L. TAN and Y. YANG, Research and Development Staff, are with the Oak Ridge National Laboratory, One Bethel Valley Road, P.O. Box 2008, MS-6151 Oak Ridge, TN 37831. Contact e-mail: yangying@ornl.gov

Manuscript submitted September 9, 2014.

Article published online December 5, 2014

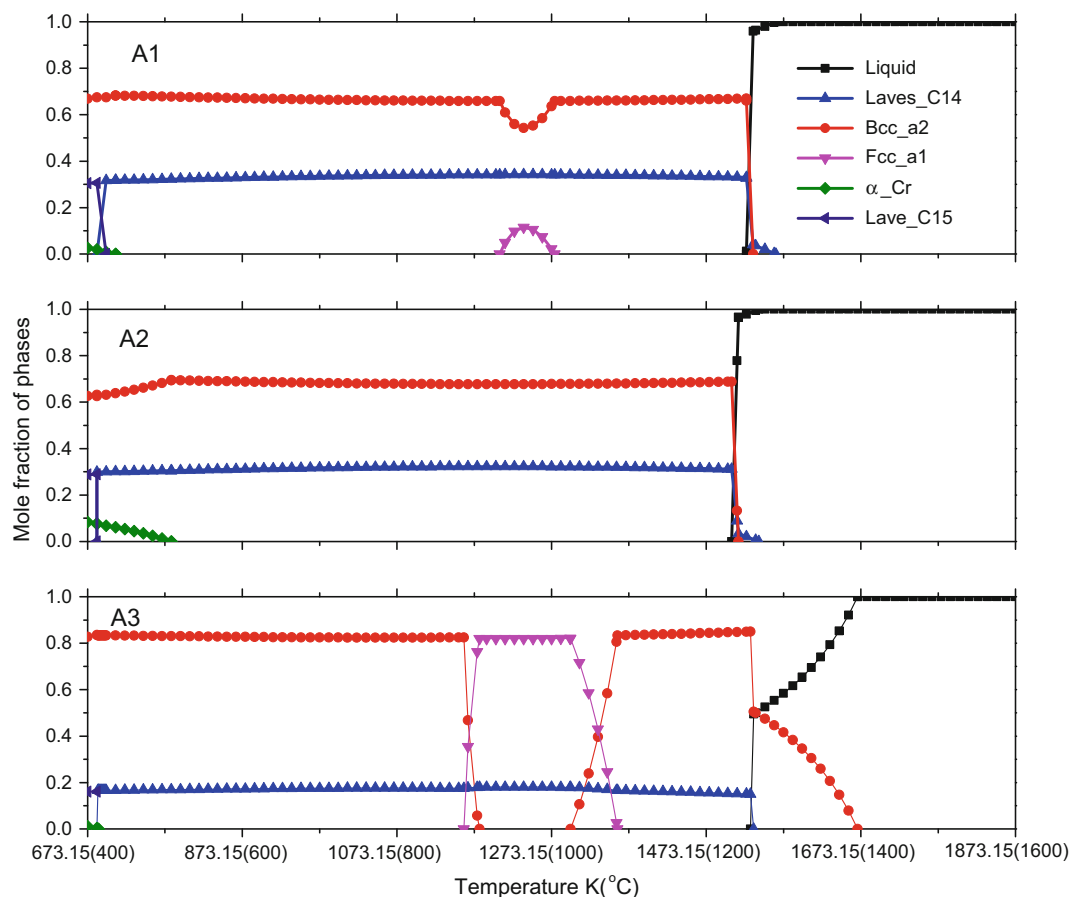


Fig. 1—Calculated temperature-dependent mole fraction of phases in alloys (a) A1:  $\text{Fe}_{81.5}\text{Cr}_9\text{Zr}_{9.5}$ , (b) A2:  $\text{Fe}_{77}\text{Cr}_{14}\text{Zr}_9$ , and (c) A3:  $\text{Fe}_{86}\text{Cr}_9\text{Zr}_5$ .

ited a good combination of room-temperature compression strength and plastic strain. However, Scudino's alloy is located in the hypereutectic region, and coarse primary Laves phase was observed in its as-cast microstructure.<sup>[11]</sup> To avoid the formation of coarse primary brittle Laves phase and promote the formation of fine dispersive Laves phase in the ductile bcc (Fe) matrix, the composition of alloy A1 was adjusted to be  $\text{Fe}_{81.5}\text{Cr}_9\text{Zr}_{9.5}$  based on thermodynamic calculation results from the recently developed thermodynamic models.<sup>[12]</sup> The calculated fractions of phases as a function of temperature in alloy A1 are shown in Figure 1(a). Its microstructure was anticipated to consist of nearly 100 pct eutectic of (bcc + Laves). To evaluate the effect of Cr and Zr on tensile properties, two other alloys, A2 and A3, were designed as  $\text{Fe}_{77}\text{Cr}_{14}\text{Zr}_9$  and  $\text{Fe}_{86}\text{Cr}_9\text{Zr}_5$ , respectively. The Zr content in alloy A2 is slightly reduced to 9 at. pct, so that it is still at the eutectic valley. The calculation suggests that alloy A2 (Figure 1(b)) has phase fractions similar to alloy A1, but with higher Cr contents in individual phases. In contrast, alloy A3 (Figure 1(c)) is located in the primary region of bcc, and its microstructure consists of primary bcc phase and eutectic of (bcc + Laves) phase, which is consistent with the finding by

Park *et al.*<sup>[10]</sup> in Fe-Zr binary alloys. Alloy A3 was anticipated to have enhanced ductility due to the increased fraction of ductile bcc phase. Transitional (bcc + fcc + Laves) three-phase region(s) was found from thermodynamic calculation for alloys A1 and A3. The region(s) was assumed to have a negligible effect on the target microstructures of the designed alloys with specified processing conditions described below.

Experimental ingots, about 500 g each, of the three alloys with their designed compositions (purity >99.95 wt pct) were prepared using arc melting and drop casting in a titanium-gettered argon atmosphere. Each alloy bottom was remelted six times in order to achieve homogeneity. The ingots were annealed at 1423.15 K (1150.15 °C) for 20 minutes followed by hot forging. Additional 10 minutes annealing was conducted on the forged materials at 1423.15 K (1150.15 °C) followed by air cooling. Partial as-processed (or as-received, AR) materials were capsuled in evacuated quartz tubes and aged at 1023.15 K (750.15 °C) for 1800 hours followed by water quench to room temperature. The aging temperature was selected based on the expected application temperature of the alloys.

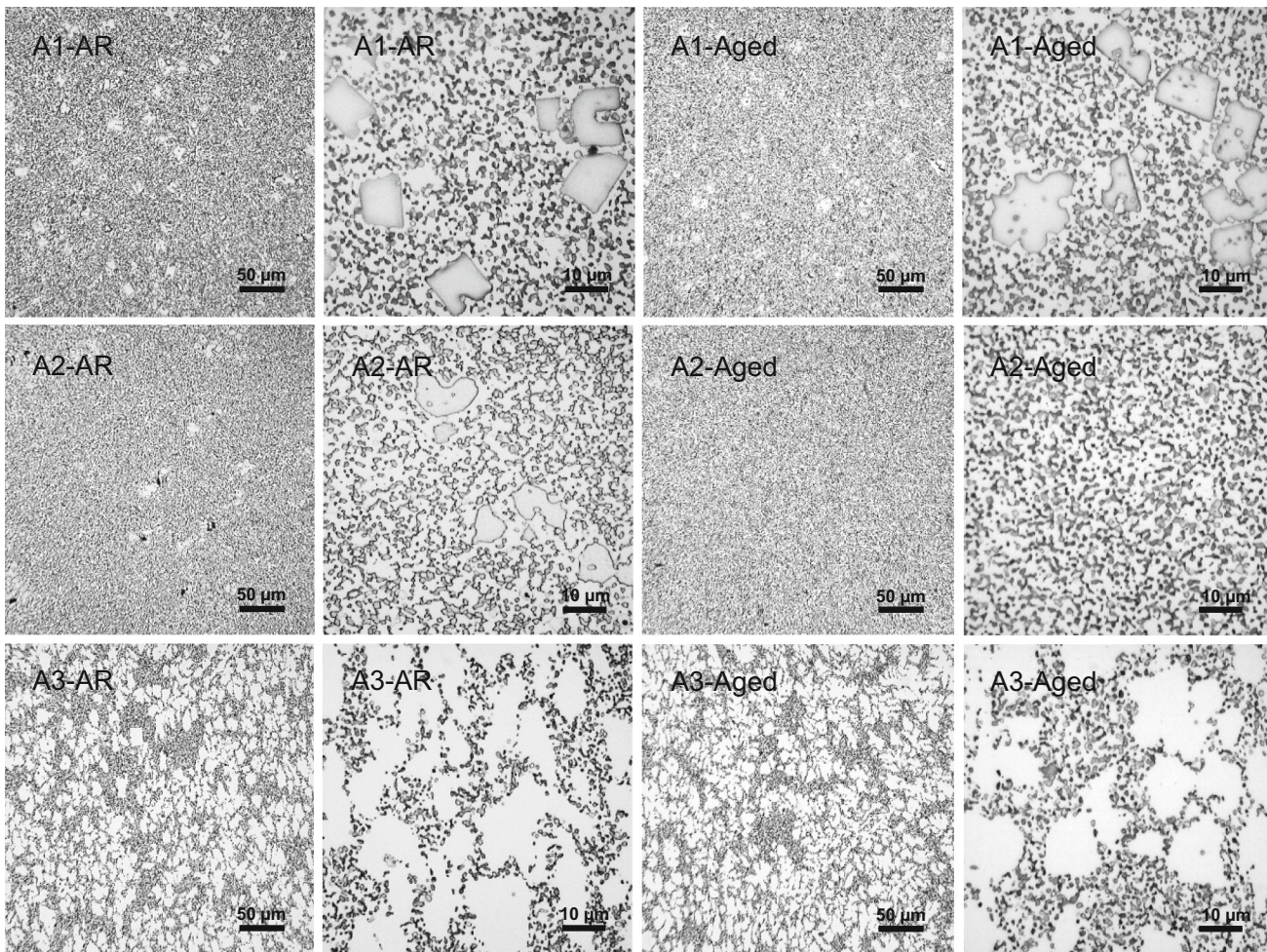


Fig. 2—Optical images ( $340 \times 340$  and  $70 \times 70 \mu\text{m}^2$ ) of alloys A1, A2, and A3 in the AR and aged conditions.

### B. Microstructural Characterization

Samples from each alloy condition were mounted in epoxy and ground using abrasive papers followed by final polishing using silica colloidal. The microstructure of the samples was examined using optical microscopy, scanning electron microscopy (SEM) primarily in backscattered electron image mode (JEOL 6500F SEM with a field emission gun), energy-dispersive X-ray spectroscopy (EDS: EDAX Apollo 40 silicon drift detector), and X-ray diffraction (XRD: PANalytical X'Pert diffractometer with a X'Celerator detector, Mo- $K\alpha$  radiation ( $\lambda = 0.709319 \text{ \AA}$ ), and 3 mm adjusting slits). The phase search and match was conducted using the Jade and/or HighScore software and the international centre for diffraction data (ICDD) powder diffraction file (PDF) database.

### C. Mechanical Testing

Mechanical properties, including hardness, tensile, and creep rupture, were conducted on the alloy samples. Vickers microhardness was measured using 1 kgf loading with 15 seconds hold time on the metallographically polished samples. Ten measurements with 0.5 mm step size between the indentations were performed on each

sample to get statistic results. Miniature specimens (type SS-3:  $25.4 \times 4.95 \times 0.76 \text{ mm}$  with a gage cross-section of  $1.52 \times 0.76 \text{ mm}$ ) were used for tensile testing and accelerated creep rupture testing. The specimens were machined with their length parallel to the longitudinal direction of the materials. Tensile testing was conducted in air at temperatures from ambient temperature up to 973.15 K (700.15 °C) using a strain rate of  $1 \times 10^{-3} \text{ s}^{-1}$  using a MTS tensile tester. To quickly and accurately control the testing temperature of the miniature specimens, a customized heating chamber was developed using a pair of infrared quartz lamps. Accelerated creep testing with shoulder load on the SS-3 specimens was conducted in air at 873 K (600 °C) and a load of 260 MPa using an ATS 2140-series direct load tester. A traditional split tube furnace was used during the creep testing.

## III. RESULTS

### A. Microstructures of the Alloys

Optical images of the AR and aged samples of alloys A1, A2, and A3 are shown in Figure 2. The images in

**Table I. EDS-measured Compositions in Atomic Percentage (at. pct) of the Features in the As-received (AR) Samples**

Alloy	Condition	Feature	Fe_K	Cr_K	Zr_L	Remark
A1	AR	matrix	87.8	11.5	0.7	
A1	AR	blocky	69.6	4.2	26.2	C36-(Fe,Cr) <sub>2</sub> Zr
A1	AR	fine	61.6	4.1	34.3	C14-(Fe,Cr) <sub>2</sub> Zr
A2	AR	matrix	81.4	17.6	1.0	
A2	AR	blocky	67.7	6.4	25.9	C36-(Fe,Cr) <sub>2</sub> Zr
A2	AR	fine	60.3	6.3	33.4	C14-(Fe,Cr) <sub>2</sub> Zr
A3	AR	matrix	89.3	10.3	0.4	
A3	AR	fine	62.9	4.2	32.9	C14-(Fe,Cr) <sub>2</sub> Zr

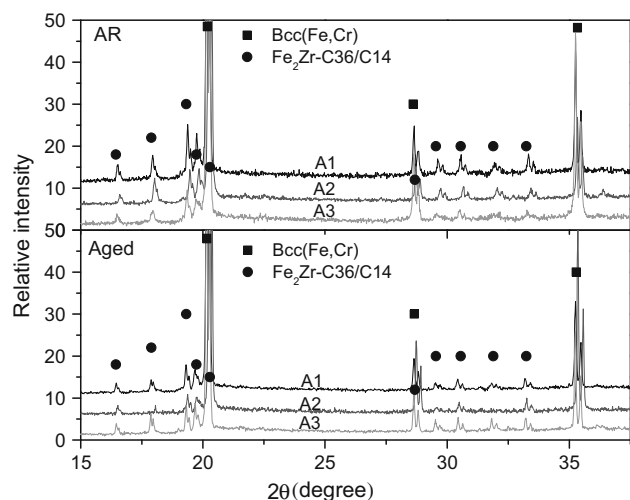


Fig. 3—XRD patterns of alloys A1, A2, and A3 in the AR and aged conditions.

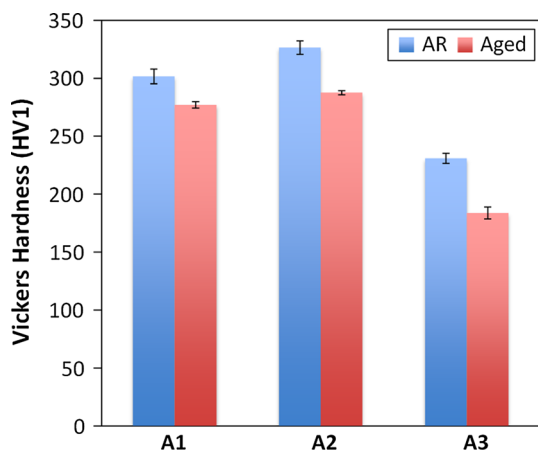


Fig. 4—Vickers microhardness of alloys A1, A2, and A3 in the AR and aged [1023.15 K (750.15 °C) for 1800 h] conditions.

the low and high magnifications reveal the overall and detailed microstructures between the alloys in different conditions, which are qualitatively consistent with the calculated results in Figure 1. Alloy A1 consists of finely distributed dark particles and a few gray blocky particles, with the former resulted from eutectic solidification and the later from primary solidification. The compositions of the features were measured using EDS

and their results are listed in Table I. Alloy A2 is also dominated with fine particles, similar to alloy A1, but has fewer blocky particles than alloy A1. Alloy A3 exhibits a distinct microstructure from A1 and A2, which has a large amount of dendritic primary phase (white) surrounded by a fine eutectic structure. The greater amount of Cr in alloy A2 resulted in higher Cr contents in the matrix as well as the fine and blocky particles as compared to those features in alloys A1 and A3. In contrast, the less amount of Zr in alloy A3 did not lead to noticeable changes to the compositions of the phases but significantly reduced the fraction of the fine particles and eliminate the presence of the blocky particles as compared to those in alloys A1 and A2. In general, the 1800 hours aging at 1023 K (750 °C) did not significantly alter the microstructures, including morphologies and phase compositions, of the alloys in the AR condition. Particle coarsening was not noticeable in the aged samples. It appears that the aging reduced the amount of the blocky particles in alloys A1 and A2, suggesting the instability of this type of phase. The less amount or the absence of blocky particles in alloy A2 indicates that the composition of A2 is very close to the eutectic composition of the alloy system.

XRD patterns of alloys A1, A2, and A3 in the AR and aged conditions are shown in Figure 3. Their patterns mainly contain peaks of bcc phase from the matrix and Laves phase from the fine and blocky particles. The Laves phase was identified as a hexagonal structure in either C36 (hP24) or C14 (hP12) structures since they are difficult to be differentiated from the XRD patterns due to the overlapping of the peaks.<sup>[12]</sup>

### B. Mechanical Properties

The Vickers microhardness data of alloys A1, A2, and A3 are summarized in Figure 4. The small error bars, denoting the standard deviation of 10 measurements on each alloy and condition, suggest good uniformity of hardness. Alloy A3 with large fraction of bcc matrix has the lowest hardness of  $230.9 \pm 4.3$  HV1. Alloys A1 and A2, with a similar amount of high-density fine eutectic Laves particles, yield similar high hardness of  $301.6 \pm 6.3$  and  $326.4 \pm 5.8$  HV1, respectively. The slightly higher hardness of A2 compared to A1 may be attributable to the higher Cr content in A2. The 1800 h aging at 1023 K (750 °C) slightly reduced the hardness of the alloys although the aging did not introduce distinct changes in microstructures as shown in Fig-

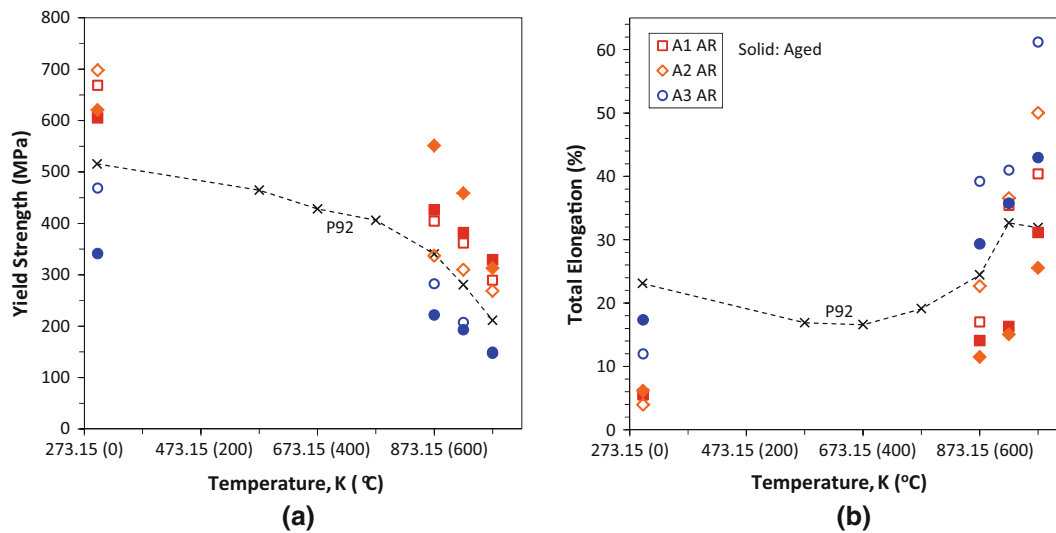


Fig. 5—Temperature-dependent (a) yield strength and (b) total elongation of alloys A1, A2, and A3 in the AR (open symbols) and aged (solid symbols) conditions compared to P92.

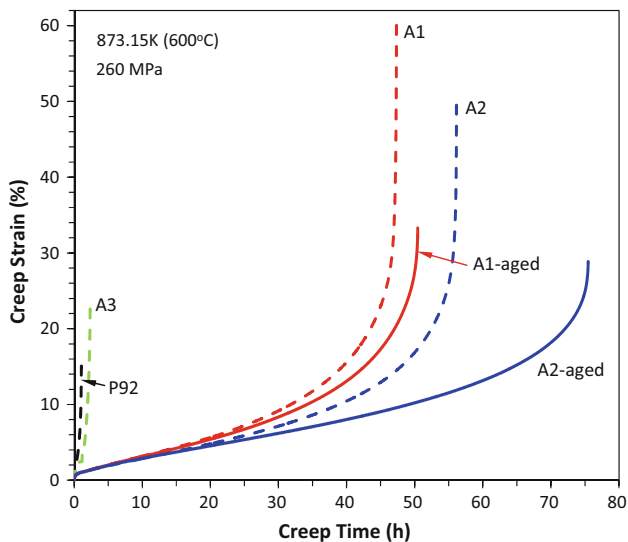


Fig. 6—Creep curves of alloys A1, A2, and A3 in the AR and aged conditions compared to P92 tested at 873.15 K (600.15 °C) and 260 MPa.

ure 2. The hardness reduction may suggest the aging-induced residual stress relaxation.

The temperature-dependent yield strength and total elongation of alloys A1, A2 and A3 are shown in Figure 5. Only one specimen was tested for each alloy at each temperature due to the limited availability of the materials. Samples of a commercial heat of P92 from Nippon Steel were tested as a reference, and the results are included in Figure 5. Consistent with the microhardness results as shown in Figure 4, alloy A2 exhibited slightly greater yield strength than A1 but noticeably greater than A3 in both the AR and aged conditions at room temperature. The strength of the alloys decreases with the increasing temperature, which approximately follows the trend of P92. While alloy A3 shows the lower strength than P92, alloys A1 and A2 in

the AR condition exhibited yield strength up to ~37 pct greater than P92. It is interesting to note that, unlike the aging-induced softening at room temperature, the aging developed greater strength at higher temperatures. The aged alloy A2 retained noticeably high strengths at 873.15 K and 923.15 K (600.15 °C and 650.15 °C), ~62 pct greater than P92. Similar to other conventional alloys, the alloys with higher strength resulted in lower total elongation or ductility as shown in Figure 5(b).

The creep curves with creep strain as a function of creep time for alloys A1, A2, and A3 in the AR (dashed lines) and aged (solid lines) conditions are shown in Figure 6, which were tested at 873 K (600 °C) and 260 MPa. The data of the commercial heat of P92 tested in this work are included for comparison. The creep testing exhibited different levels of improvement in creep resistance of the alloys in both creep life and ductility over P92. Alloy A3 had a comparable creep life but noticeably greater creep strain than P92. In contrast, alloys A1 and A2 developed significant enhancement in both creep life and creep strain, *e.g.*, 47.3 hours creep life and 60.2 pct creep strain of A1 vs 1.1 hours and 15.5 pct of P92. Similar to the aging-induced strengthening and ductility reduction, the aging resulted in further improvement in creep life but with reduced creep strain for both A1 and A2. Unlike the inferior total elongations compared to P92 at 873 K (600 °C) as shown in Figure 5(b), the creep strains of A1 and A2 (~29 to 60 pct) were noticeably higher than P92 at 873 K (600 °C). It suggests that alloys A1 and A2 are capable of being used in low-strain-rate conditions. Due to the aging-induced softening to alloy A3 as shown in Figure 5(a), the creep testing resulted in reduced creep life that is not shown in Figure 6.

### C. Fractography

The fractography of the tensile- and creep-tested samples was characterized using SEM and EDS. Fig-

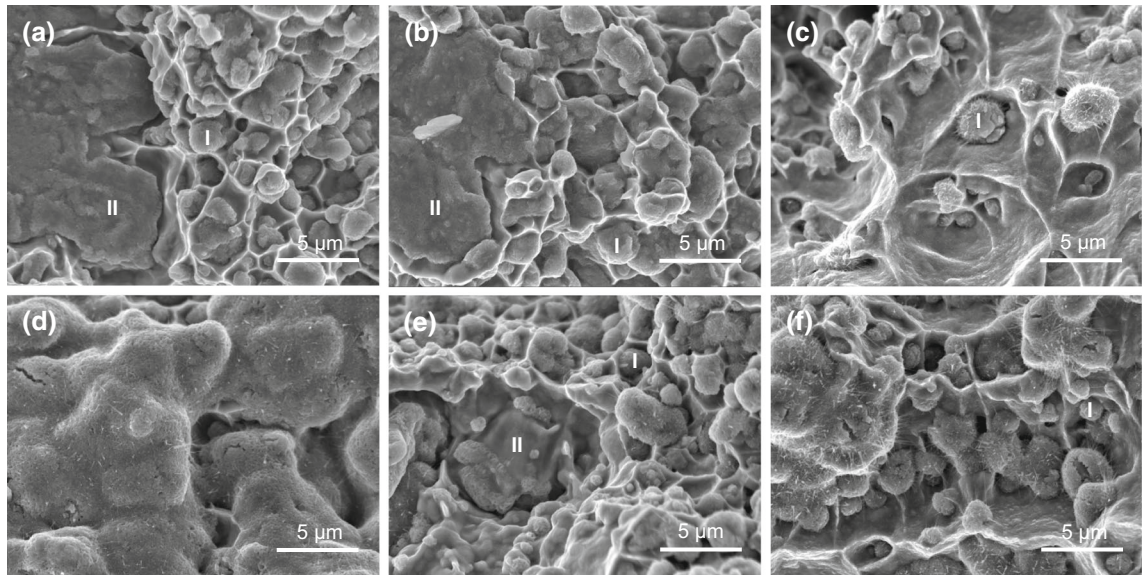


Fig. 7—Typical fracture surface morphologies of the tensile-tested (a) A1, (b) A2, and (c) A3 samples at 873.15 K (600.15 °C) and the creep-tested (d) A1, (e) A2, and (f) A3 samples at 873.15 K (600.15 °C) and 260 MPa.

Figure 7 shows the typical fracture surface morphologies of the alloy samples tested at 873.15 K (600.15 °C) under tensile and creep conditions. Oxidation occurred on both the tensile- and creep-tested samples. The oxidation of the tensile-tested samples occurred during the fracture and the subsequent air cooling to room temperature, which took less than ~0.5 hour. In contrast, the creep-tested samples were furnace cooled from 873.15 K (600.15 °C) after the rupture of the samples, which took ~8 hours. Therefore, the fractography of the tensile-tested samples is considered to be more close to the fresh fracture surface.

Alloys A1 and A2 (Figures 7(a) and (b), respectively) exhibited mixed ductile and brittle fracture morphologies after tensile testing at 873 K (600 °C), while alloy A3 shows a typical ductile fracture morphology, as shown in Figure 7(c) featured with microvoids and dimples in the bcc matrix. Correlating with the microstructures in the AR condition as shown in Figure 2, the fine Laves particles, labeled with I, served as nucleation sites of dimples of the ductile fracture. Cleavage fracture primarily occurred in the blocky Laves particles, labeled with II, in alloys A1 and A2. Similar morphologies were observed on the room-temperature tensile-tested samples. The thin layer of bcc matrix ligament between the fine particles in alloys A1 and A2 does not have enough plastic deformation capacity, resulting in low total elongations at room temperature. Although alloy A3 has a large amount of bcc matrix, yielding a decent total elongation at room temperature, the bcc matrix does not have enough strength as illustrated in Figure 5(a).

The creep-fractured surface morphologies, as shown in Figures 7(d) through (f), are similar to the tensile-fractured morphologies, except for the extensive oxidation. Disregarding the complicated oxidation behavior that will be studied separately, the fractography of the tensile and creep testing indicates that the samples were

primarily ductile fracture with some cleavage-type brittle fracture in the blocky phase.

#### IV. DISCUSSION

The fractography results suggest the cleavage fracture is primarily occurred in the blocky Laves particles, while the fine Laves particles served as nucleation sites of dimples of the ductile fracture. Therefore, it is necessary to know what these Laves particles are. It has been described earlier that C14 and C36 Laves phases co-exist in the microstructure. The XRD was not able to identify one from the other due to the overlapping diffraction peaks. The EDS measurements on individual phases in Figure 2 suggested that the Zr concentration in the fine Laves phase is more close to the stoichiometric ratio of 33.3 at. pct, while that in the blocky Laves phase it is ~26 at. pct, as shown in Table I. To identify whether the blocky phase is the C36 or C14 structure, a detailed lattice parameter analysis is carried out. The  $a$  and  $c$  parameters from the dominant XRD peaks of the Laves phase are calculated in the ranges of 4.91-4.97 and 8-8.1 Å, respectively. The calculated lattice parameters are in good agreement with the C14 structure of the Laves phase in literature.<sup>[13,14]</sup> Since the fine Laves phase has larger volume fraction than the blocky one, it is reasonable to conclude the fine Laves phase has the C14 structure, while the blocky one has the C36 structure. The measured lattice parameter is plotted against the Fe content in the C14 Laves phase in Figure 8. The calculated lattice parameters ( $a$  and  $c$ ) were found to be dependent upon Fe content of the alloys as shown in Figure 8(b). Greater Fe content tends to have greater lattice parameters for both  $a$  and  $c$ . The aging led to slight increases of the lattice parameters.

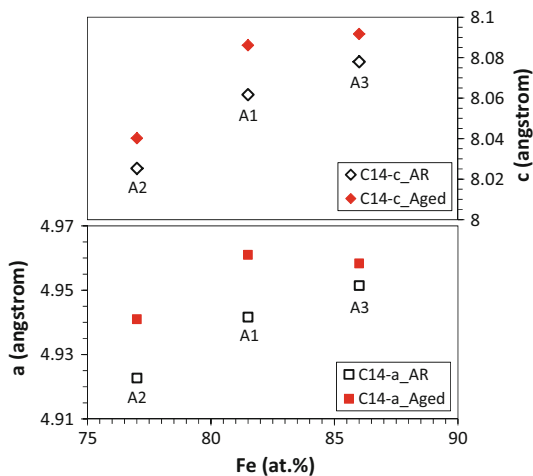


Fig. 8—Analyzed lattice parameters of the C14-Laves phase in the AR (open symbols) and aged (solid symbols) conditions.

According to the thermodynamic calculations, the 5 at. pct Cr increase in alloy A2 compared to that in A1 results in slight decreases in fine Laves phase (~2 pct mole fraction) and blocky Laves primary phase (~0.6 pct mole fraction) that was noticed during microstructural characterization as shown in Figure 2. Measurable increases in Cr content were found in the bcc matrix (~6 at. pct) and Laves phase (~2 at. pct) of alloy A2. It seems that such small changes induced by the increased Cr content tended to increase strength but reduce ductility of the alloy. This observation under tensile condition is different from the increased ductility by increasing Cr content under compression condition at room temperature.<sup>[11]</sup> The 4.5 pct Zr reduction in alloy A3 compared to that in A1 resulted in significant reduction in fine Laves phase and increase in coarse bcc primary phase, which resulted in deformation primarily occurring in the coarse bcc primary phase. According to the fractography result, tuning alloy compositions to eliminate the blocky Laves primary phase and increase an appropriate amount of bcc matrix in A1 and A2 (or reduce the amount of bcc matrix in A3) would yield an optimum alloy with desired strength and ductility combinations.

The excellent strength of alloys A1 and A2 showed lower total elongations, *e.g.*, ~6 pct at room temperature and ~20 pct at temperatures below 923.15 K (650.15 °C). The low ductility may limit the applications of the alloys at relatively low temperatures under tensile condition. However, they may be applicable to compression condition as suggested by the Fe-10Cr-10Zr alloy with a reported plastic strain of ~17 pct under compression testing at room temperature.<sup>[11]</sup>

## V. CONCLUSIONS

Three Fe-Cr-Zr alloys were designed to favor the formation of fine eutectic structure containing Laves phase. Two alloys, Fe<sub>81.5</sub>Cr<sub>9</sub>Zr<sub>9.5</sub> (A1) and Fe<sub>77</sub>Cr<sub>14</sub>Zr<sub>9</sub> (A2), were about right on the eutectic point with trace

amounts of Laves phase as primary phase. The other alloy, Fe<sub>86</sub>Cr<sub>9</sub>Zr<sub>5</sub> (A3), was away from the eutectic point with about 50 pct of bcc as primary phase. Microstructural characterization using optical microscopy, SEM/EDS, and XRD confirmed the phase components and compositions that are consistent with the thermodynamic calculations. The Laves phase was identified as C14- and C36-types, presented as fine and blocky particles, respectively.

Samples of the alloys were subjected to Vickers hardness measurements at room temperature, tensile testing at temperatures up to 973.15 K (700.15 °C), and creep testing at 873.15 K (600.15 °C) with 260 MPa load. Alloy A2 exhibited slightly higher hardness and strength than A1, but noticeably higher than A3. The strength of alloys A1 and A2 was significantly superior to P92 at the tested temperatures. However, their ductility was noticeably lower, especially at lower temperatures. Despite the low tensile ductility, alloys A1 and A2 showed remarkably high ductility, together with great creep life, during the creep testing. The results suggest that alloys A1 and A2 are capable of being used at high temperatures, *e.g.*, ~873.15 K (600.15 °C) and above. Alloy A3 had inferior tensile performance but comparable creep resistance to P92. Thermal aging at 1023.15 K (750.15 °C) for 1800 hours did not significantly alter the microstructures but decreased the strength of alloys A1 and A2 with increases in ductility at room temperature, which were in contrary to those at elevated temperatures. Fractography analysis indicated primarily ductile fracture of the samples. Some isolated cleavage-type brittle fracture occurred at blocky Laves primary phase in alloys A1 and A2. The 5 at. pct Cr increase in alloy A2 did not introduce significant changes compared to A1. In contrast, the 4.5 at. pct Zr decrease in alloy A3 resulted in significant reduction in Laves phase and increase in coarse bcc primary phase, leading to remarkably lower strength and creep resistance. The results indicate that appropriate composition adjustment would yield a desired strength and ductility combination.

## ACKNOWLEDGMENTS

This research was supported by the U.S. Department of Energy (DOE), Office of Nuclear Energy, Nuclear Engineering Enabling Technology (NEET) Advanced Reactor Material Program, under contract DE-AC05-00OR22725 with UT-Battelle, LLC, and through a user project supported by ORNL's Center for Nanophase Materials Sciences (CNMS) that was sponsored by the Scientific User Facilities Division, Office of Basic Energy Sciences, U.S. DOE.

## REFERENCES

1. N. Baluc, R. Schaeublin, P. Spaetig, and M. Victoria: *Nucl. Fus.*, 2004, vol. 44, pp. 56–61.
2. H. Mimura, M. Ohgami, H. Naoi, and T. Fujita: in *Materials for Advanced Power Engineering*, D. Coutsouradis, ed., Kluwer Academic Publishers, The Netherlands, 1994.

3. B. Raj and M. Vijayalakshmi: in *Comprehensive Nuclear Materials*, R.J.M. Konings, et al., ed., Elsevier, Amsterdam, 2012.
4. T. Allen and D. Crawford: *Science and Technology of Nuclear Installations*, 2007.
5. K. Maruyama, K. Sawada, and J.-I. Koike: *ISIJ Int.*, 2001, vol. 41, pp. 641–53.
6. J.D. Livingston: *Phys. Status Solidi A*, 1992, vol. 131, pp. 415–23.
7. A. Wasilkowska, M. Bartsch, F. Stein, M. Palm, G. Sauthoff, and U. Messerschmidt: *Mater. Sci. Eng. A*, 2004, vol. A381, pp. 1–15.
8. A. Wasilkowska, M. Bartsch, F. Stein, M. Palm, K. Sztwiertnia, G. Sauthoff, and U. Messerschmidt: *Mater. Sci. Eng. A*, 2004, vol. A380, pp. 9–19.
9. Y. Liu, J.D. Livingston, and S.M. Allen: *Metall. Trans. A*, 1992, vol. 23A, pp. 3303–08.
10. J.M. Park, S.W. Sohn, T.E. Kim, D.H. Kim, K.B. Kim, and W.T. Kim: *Scripta Mater.*, 2007, vol. 57, pp. 1153–56.
11. S. Scudino, P. Donnadieu, K.B. Surreddi, K. Nikolowski, M. Stoica, and J. Eckert: *Intermetallics*, 2009, vol. 17, pp. 532–39.
12. Y. Yang, L. Tan, H. Bei, and J.T. Busby: *J. Nucl. Mater.*, 2013, vol. 441, pp. 190–202.
13. S. Kuranaka, T. Gamo, and Y. Morita: *J. Alloy. Compd.*, 1997, vol. 253, pp. 268–71.
14. J. Soubeyroux, M. Bououdina, D. Fruchart, and L. Pontonnier: *J. Alloy. Compd.*, 1995, vol. 219, pp. 48–54.